Article

Cell Reports

CXCR4 Regulates Extra-Medullary Myeloma through Epithelial-Mesenchymal-Transition-like Transcriptional Activation

Graphical Abstract

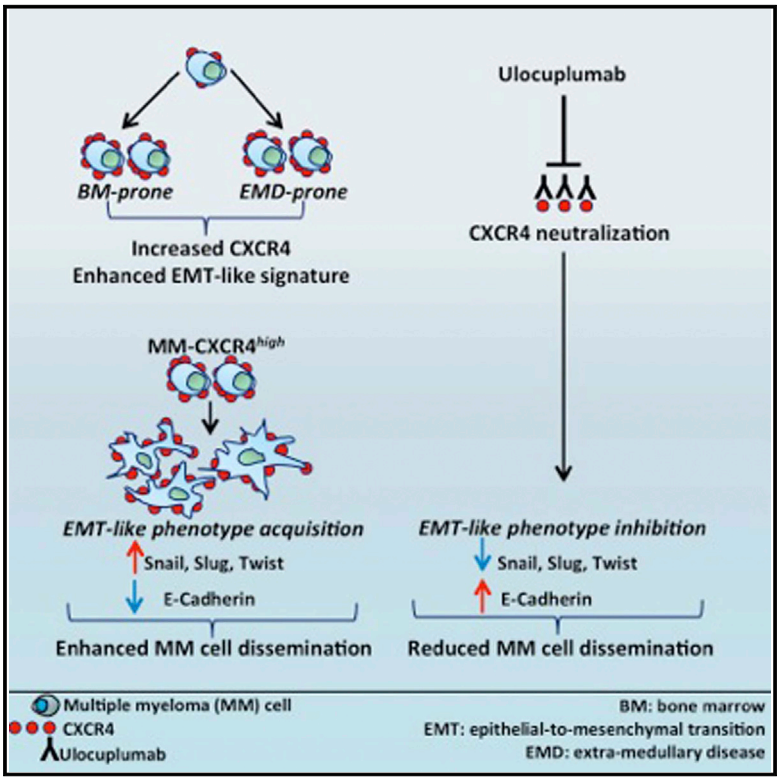

Highlights

- CXCR4 mediates extra-medullary multiple myeloma (MM)
- CXCR4 enhances EMT-like phenotype acquisition in MM
- Ulocuplumab inhibits MM cell dissemination and EMT acquisition in MM

Authors

Aldo M. Roccaro, Yuji Mishima, Antonio Sacco, ..., Pina Cardarelli, Michelle Kuhne, Irene M. Ghobrial

Correspondence

irene_ghobrial@dfci.harvard.edu

In Brief

Roccaro et al. report on the role of CXCR4 in inducing acquisition of an EMT-like signature in MM cells, demonstrate that CXCR4 may act as a regulator of EMD through EMT-like transcriptional modulation, and indicate CXCR4 as a potential therapeutical target to prevent MM disease progression.

Accession Numbers

GSE68538
GSE24080
GSE6477

Roccaro et al., 2015, Cell Reports *12*, 622–635
July 28, 2015
http://dx.doi.org/10.1016/j.celrep.2015.06.059

OPEN ACCESS
CellPress

Cell Reports
Article

CXCR4 Regulates Extra-Medullary Myeloma through Epithelial-Mesenchymal-Transition-like Transcriptional Activation

Aldo M. Roccaro,[1,9] Yuji Mishima,[1,7,9] Antonio Sacco,[1,9] Michele Moschetta,[1] Yu-Tzu Tai,[1] Jiantao Shi,[2,3] Yong Zhang,[1] Michaela R. Reagan,[1,8] Daisy Huynh,[1] Yawara Kawano,[1] Ilyas Sahin,[1] Marco Chiarini,[1,4] Salomon Manier,[1] Michele Cea,[1] Yosra Aljawai,[1] Siobhan Glavey,[1] Elizabeth Morgan,[5] Chin Pan,[6] Franziska Michor,[2,3] Pina Cardarelli,[6] Michelle Kuhne,[6] and Irene M. Ghobrial[1,*]

[1]Department of Medical Oncology, Dana-Farber Cancer Institute, Harvard Medical School, Boston, MA 02215, USA
[2]Department of Biostatistics and Computational Biology, Dana-Farber Cancer Institute, Boston, MA 02215, USA
[3]Department of Biostatistics, Harvard T.H. Chan School of Public Health, Boston, MA 02215, USA
[4]Spedali Civili di Brescia, Centro per la Ricerca Onco-ematologica AIL (CREA), 25123 Brescia, Italy
[5]Department of Pathology, Brigham & Women's Hospital, Boston, MA 02215, USA
[6]Bristol-Myers Squibb, Redwood City, CA 94063, USA
[7]Cancer Chemotherapy Center, Japanese Foundation for Cancer Research, Tokyo 135-8550, Japan
[8]Maine Medical Center Research Institute (MMCRI), Scarborough, ME 04074, USA
[9]Co-first author
*Correspondence: irene_ghobrial@dfci.harvard.edu
http://dx.doi.org/10.1016/j.celrep.2015.06.059

SUMMARY

Extra-medullary disease (EMD) in multiple myeloma (MM) is associated with poor prognosis and resistance to chemotherapy. However, molecular alterations that lead to EMD have not been well defined. We developed bone marrow (BM)- and EMD-prone MM syngeneic cell lines; identified that epithelial-to-mesenchymal transition (EMT) transcriptional patterns were significantly enriched in both clones compared to parental cells, together with higher levels of CXCR4 protein; and demonstrated that CXCR4 enhanced the acquisition of an EMT-like phenotype in MM cells with a phenotypic conversion for invasion, leading to higher bone metastasis and EMD dissemination in vivo. In contrast, CXCR4 silencing led to inhibited tumor growth and reduced survival. Ulocuplumab, a monoclonal anti-CXCR4 antibody, inhibited MM cell dissemination, supported by suppression of the CXCR4-driven EMT-like phenotype. These results suggest that targeting CXCR4 may act as a regulator of EMD through EMT-like transcriptional modulation, thus representing a potential therapeutic strategy to prevent MM disease progression.

INTRODUCTION

The process of tumor cell metastasis is a multilevel phenomenon, which involves several steps including cell invasion, blood vessel intravasation, and passage of the tumor cells into the circulation, followed by homing or extravasation of the clonal cells into distant tissues, resulting in the formation of new foci of tumor colonization. Multiple myeloma (MM) represents a plasma cell dyscrasia characterized by the presence of clonal plasma cells within the bone marrow (BM), together with multiple myelomatous "omas" throughout the skeleton. The occurrence of bone lytic lesions suggests a continuous trafficking of tumor cells to multiple BM areas. A subset of MM patients may present with extra-medullary disease (EMD), defined as an infiltrate of clonal plasma cells at an anatomic site distant from the BM. EMD occurs in about 4%–20% of patients with MM either at the time of diagnosis or more frequently after multiple relapses (Oriol, 2011; Varettoni et al., 2010; Weinstock and Ghobrial, 2013). Prior clinical observations have shown that patients with EMD have a poor prognosis with a median overall survival of 1.3 years from the time of diagnosis of EMD (Weinstock and Ghobrial, 2013). A recent study has reported on the incidence and clinical features of EMD in MM patients (Weinstock et al., 2015). However, the mechanisms by which EMD occurs in MM and whether it can be therapeutically targeted to improve the survival of these patients remain poorly explored.

Epithelial-mesenchymal transition (EMT) programs occur in both physiological conditions, such as during implantation, embryogenesis, and organ development (type-1 EMT; Acloque et al., 2009; Vićovac and Aplin, 1996) and in pathological settings, including tissue regeneration and fibrosis (type-2 EMT; Okada et al., 1997; Zeisberg et al., 2007a, 2007b) as well as cancer progression and metastasis (type-3 EMT; Ansieau et al., 2008; Brabletz et al., 2001; Gupta et al., 2005; Hanahan and Weinberg, 2000; Medici et al., 2008; Smit and Peeper, 2008; Thiery, 2002; Yang et al., 2006; Yang and Weinberg, 2008). We previously demonstrated that EMT-like transcriptional regulation occurs in MM cells during hypoxic conditions (Azab et al., 2012a). However, whether EMT plays a role in regulating MM cell dissemination and EMD remains unexplored.

Among the factors that may modulate metastasis in the context of solid tumors, CXCR4 and its ligand CXCL12 have been reported to act as positive regulators of tumor cell metastasis (Müller et al., 2001; Orimo et al., 2005; Schioppa et al., 2003; Yagi et al., 2011). CXCL12 axis has been reported to play a crucial role in facilitating BM homing and engraftment of clonal MM plasma cells, thus resulting in enhanced MM cell dissemination from bone-to-bone (Roccaro et al., 2014). Here, we found that an EMT-like signature characterizes both EMD as well as MM disease progression in a human MM cell line propagated in vivo to develop EMD and BM-prone cells. Similar results were observed in patient samples during disease progression with higher CXCR4 expression at the protein level and a higher EMT-like signature at the transcriptional level. We subsequently interrogated whether CXCR4 may enhance a metastatic-prone phenotype in MM cells in vivo by favoring EMT-like features within the tumor clone. We dissected the in vivo functional relevance of CXCR4 in mediating the EMT-related signature as well as MM cell dissemination, tumor growth, and survival by using gain- and loss-of-function approaches. We next tested the anti-metastatic activity of the monoclonal antibody anti-CXCR4 (ulocuplumab) in vivo, in the context of both MM, confirming the ability of ulocuplumab to modulate the expression of EMT-related genes. Overall, our findings support the preclinical evidence for targeting CXCR4 as a novel approach to inhibit tumor cell metastasis through the regulation of EMT.

RESULTS

EMT-like Transcriptional Regulation Characterizes Extra-Medullary MM

To examine molecular alterations that occur in EMD, we generated EMD- and BM-prone MM cells by adopting a serial in vivo selection approach (Figure S1A). After three rounds of in vivo selections, the total number of human MM cells engrafted to femur-BM and liver was calculated for the BM-prone and EMD-prone MM cell lines by counting GFP+ cells from the BM-harvested cells and from the collagenase-digested liver, respectively. Localization of the BM- and EMD-prone cells was examined using a fluorescence microscope on the whole transparent CUBIC-treated mouse (Figure 1A). Specifically, both the BM- and the EMD-clone colonized BM niches, including vertebrae, humeri, tibiae, and femurs; in addition, the EMD-clone could metastasize to and engraft within extra-medullary sites, including liver, kidney, and abdominal-pelvic areas, whereas extra-medullary infiltration of the BM-prone clone was not detectable (Figure 1B). A representative 3D reconstruction of BM and liver infiltration of BM- and EMD/liver-prone MM cells is provided (Figure 1C). The number of liver-infiltrating MM.1S cells was higher after injection of the EMD-prone clone compared to the BM-prone clone (Figures S1B and S1C). There were no significant differences in the number of BM-infiltrating cells between the EMD- and BM-prone clones (Figure S1D), thus confirming that the EMD-prone MM.1S clone presents with enhanced ability of liver homing, together with an equivalent infiltrative ability within the BM, compared to the BM-prone counterpart. In addition, the two clones did not differ in terms of cell proliferation. Moreover, both the BM- and the EMD-prone clones significantly enhanced their migration in response to the chemoattractant, with the EMD-prone clone presenting with higher migration as compared to the BM-prone clone (Figures S1E and S1F).

We next performed RNA sequencing on the BM- and EMD-prone clones and compared their transcriptional profile to the parental MM.1S cells. We found that the most significantly enriched mRNA signatures in EMD- and BM-prone clones included genes defining an epithelial-mesenchymal transition (EMT), genes upregulated in response to hypoxia, and genes related to TNFα/NFkB response, as shown by GSEA (Figure 1D; Tables S1 and S2). These findings, therefore, indicate that EMT occurs in BM-disseminating MM cells but also in MM cells colonizing EMD sites, such as the liver.

It is known that CXCR4 may act as a positive regulator of tumor cell metastasis, and previous studies have shown that EMT regulates CXCR4, leading to enhanced metastasis and cell dissemination in solid tumors (Müller et al., 2001; Orimo et al., 2005; Schioppa et al., 2003; Yagi et al., 2011). MM cells have been previously shown to express CXCR4 and this has been linked to the BM homing, engraftment, and growth of the clonal plasma cells (Alsayed et al., 2007), and we have previously shown that hypoxia may enhance CXCR4 expression in MM (Azab et al., 2012a). We therefore hypothesized that CXCR4 may be upregulated with the acquisition of an EMT-like phenotype during disease progression and development of EMD in MM, thus resulting in an enhanced MM cell dissemination. We therefore evaluated the expression pattern of CXCR4 at the protein level and confirmed that both BM- and EMD-prone clones expressed higher surface CXCR4 by flow cytometry, compared to the parental cells, with a relatively higher expression in the EMD-prone cells compared to the BM-prone cells (Figure S1G). Importantly, these findings were recapitulated using patient-derived EMD tissues, including brain, breast, liver, and abdominal wall mass, where a positivity for CXCR4 was demonstrated in CD138+ cell-infiltrated areas (Figure 1E). The expression of other chemokine receptors was tested, showing minimal differences between the BM- and the EMD-prone clones (Figure S1H).

EMT-like Phenotype Acquisition in Patient Samples with MM during Disease Progression

We next examined whether an EMT signature is also present in patient BM-derived CD138$^+$ cells. We therefore investigated the publically available gene sets (GSE24080), classified patients according to the International Staging System (ISS) (Greipp et al., 2005), and confirmed a significant enrichment for EMT-related mRNA signature in ISS1- versus ISS3-MM patients. Similarly, an EMT-like phenotype was demonstrated, evaluating an independent gene set (GSE6477) in active MM compared to smoldering MM patients, as well as in relapsed MM patients (Figures 2A and 2B). To further investigate whether CXCR4 may favor the acquisition of an EMT-like signature in MM cells, we categorized primary BM-MM-derived CD138 cells according to their CXCR4 expression levels. Patients with higher (log fold change > 1.1) and lower CXCR4 expression (log FC < -1) were next examined (Figure S2A). We first adopted a positive control gene set, represented by a signature of genes activated by

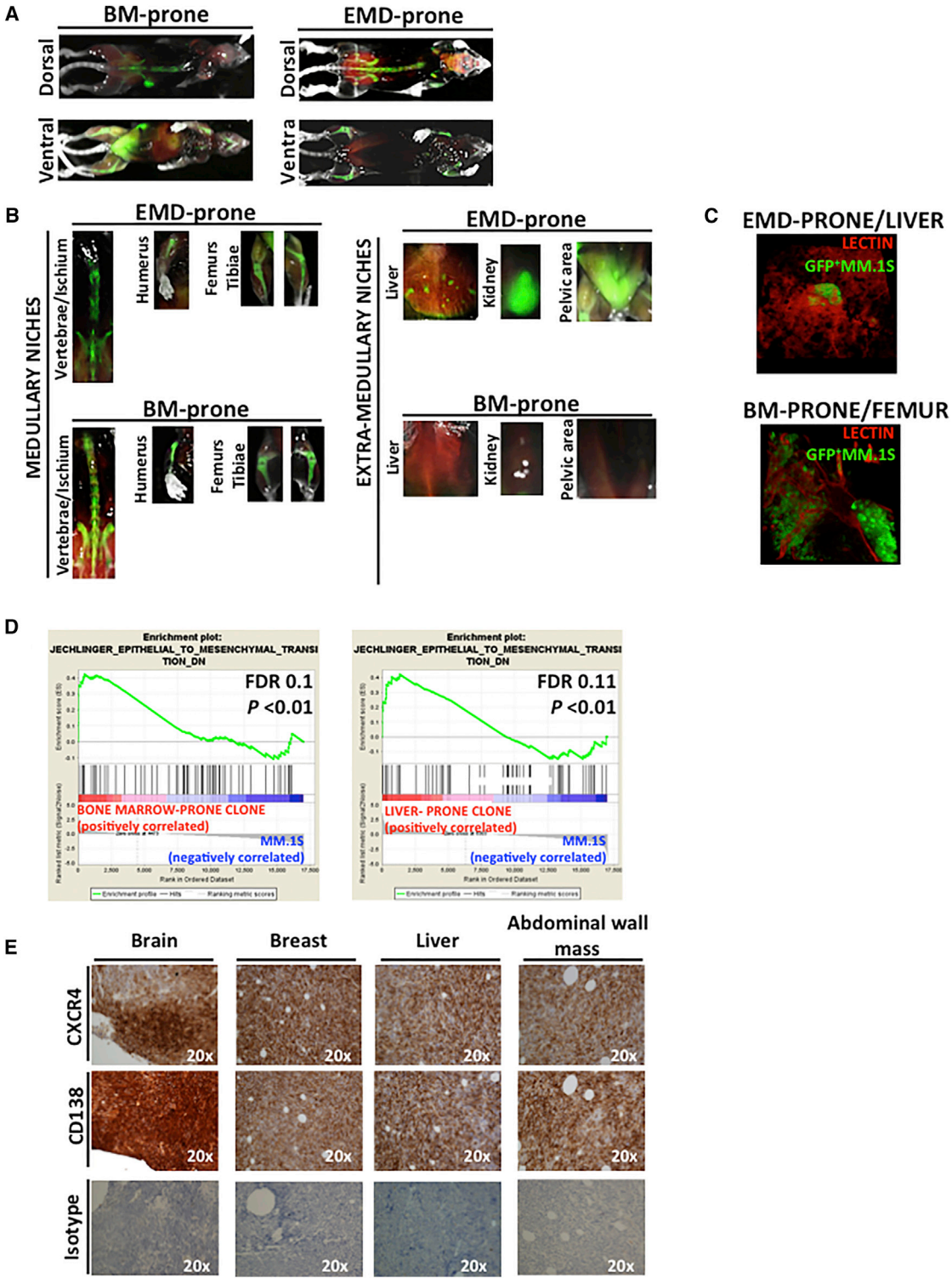

Figure 1. RNA Sequencing Shows Enrichment for Epithelial-to-Mesenchymal Transition Signature in Bone-Marrow- and Liver-Prone MM Cells

(A and B) BM-prone and liver-prone MM.1S/GFP+ cell lines were developed by serial in vivo selection as described within Figure S1. BM- and liver-prone clones were injected i.v. into SCID/Bg mice (n = 3/group). Visualization of BM- and liver-colonizing MM cells was documented by fluorescence microscopy using transparent CUBIC-treated whole-mouse body.

(legend continued on next page)

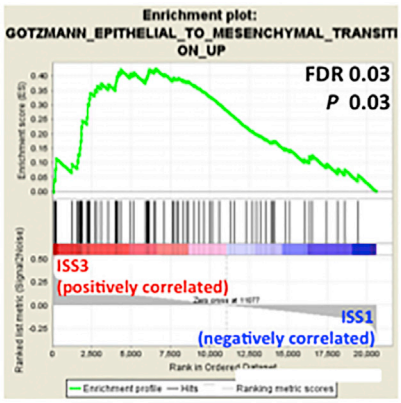

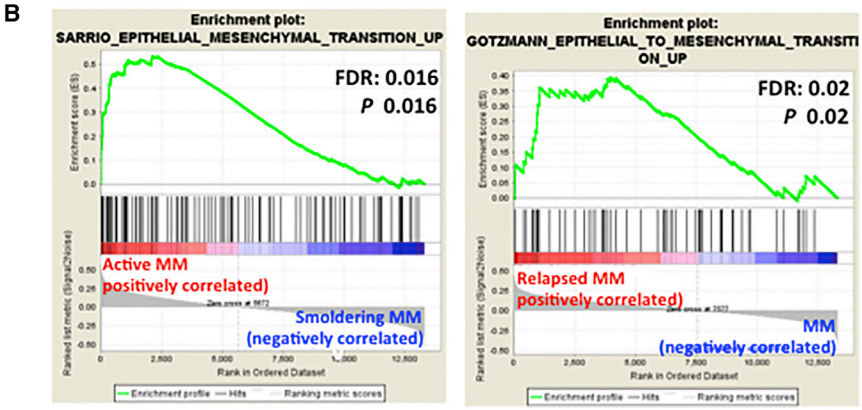

Figure 2. EMT Characterizes MM Patients with Advance Stage Disease

(A) MM patients (GSE24080) with ISS3 presented with an enrichment for EMT-like mRNA signature, compared to MM patients with ISS3, as shown by GSEA.

(B) MM patients (GSE6477) with active MM presented with an enrichment for EMT-like mRNA signature, compared to patients with smoldering MM. Similarly, an enrichment for EMT-like mRNA signature was observed in relapsed MM patients, as shown by GSEA.

CXCR4 (CXCR4_OE; instance ID OEB005_HT29_96H: BRDN0000410050) and confirmed an enrichment of the CXCR4_OE signature in patients characterized by higher CXCR4 expression versus patients with lower CXCR4 expression, as shown by using GSEA (FDR 0.1; p = 0.01; Figure S2B). We further proceeded to identify the pathways differentially expressed between BM-MM CD138^{+} plasma cells with high CXCR4 expression (MM-CXCR4^{high}), compared to clonal MM plasma cells with lower CXCR4 expression (MM-CXCR4^{low}), by using GSEA and observed an EMT-related pathway to be significantly enriched in MM- CXCR4^{high} versus MM-CXCR4^{low} (FDR 0.026; p = 0.01; Table S3). These findings further suggest that CXCR4 may possibly modulate EMT in the context of MM.

CXCR4 Regulates the Acquisition of an EMT-like Phenotype in MM

To date, several studies have shown that EMT leads to CXCR4 upregulation, leading to enhanced tumor cell dissemination (Jung et al., 2013; Müller et al., 2001). However, we sought to examine whether, conversely, CXCR4 may regulate the EMT-like transcriptional regulation in MM using in vivo models. We first performed CXCR4 gain-of-function studies and confirmed that CXCR4 overexpression led to the acquisition of a mesenchymal-like morphology, with changes in actin cytoskeleton reorganization of MM cells with protrusion of cell pseudopodia, compared to empty vector (EV)-infected cells (Figure 3A). This phenotype was also supported by the modulation of EMT-related markers in CXCR4-overexpressing (CXCR4/OE) MM.1S cells compared to EV-infected cells, as shown by upregulation of Slug, Snail, and Twist, together with downregulation of E-cadherin (Figure 3B). Of note, CXCR4/OE cells also showed enhanced activation of pro-survival pathways, such as p-ERK and p-AKT, together with modulation of migration and adhesion-related proteins (Figure 3B). In addition, CXCR4/OE MM cells presented with enhanced invasive properties compared to control cells (Figure 3C). Demonstration of CXCR4 overexpression in CXCR4/OE MM cells compared to EV-infected cells was performed using qRT-PCR and western blot (Figures 3B and S3A). Similarly, additional MM cell lines (RPMI.8226) presented with the same changes in cellular morphology, together with enhanced Slug, Snail, and Twist

(C) GFP-expressing BM- and EMD-prone MM1.S cells were visualized within the resected BM and liver, respectively, using transparent CUBIC-treated femur and liver and reconstructed in 3D using z stack images. GFP expression (green signal) indicates myeloma cells; blood vessels were labeled with DyLight 594 conjugated Lycopersicon Esculentum Lectin (red signal).

(D) BM- and liver-prone MM.1S cells were subjected to RNA sequencing, showing an enrichment for EMT-related mRNA signature, as shown by performing GSEA. The green curves show the enrichment score and reflect the degree to which each gene (black vertical lines) is represented at the top or bottom of the ranked gene list. The heatmap indicates the relative abundance (red to blue) of the genes specifically enriched in the BM- or liver-prone MM.1S cells as compared to original MM.1S cells. EMT gene sets were enriched in the BM- and in the liver-prone MM.1S cells.

(E) Expression of CXCR4 on samples obtained from patients with extra-medullary MM, including brain, breast, liver, and abdominal wall mass, was evaluated by immunohistochemistry using anti-CXCR4 antibody. Staining for CD138 was also performed to identify the MM-infiltrating areas. Isotype control was used for the EMD tissues stained for CXCR4 and CD138. Immunohistochemistry images were obtained from brain, breast, liver, and abdominal wall. Tissues were visualized with an Eclipse 80i microscope (Nikon); 20× magnifications are provided.

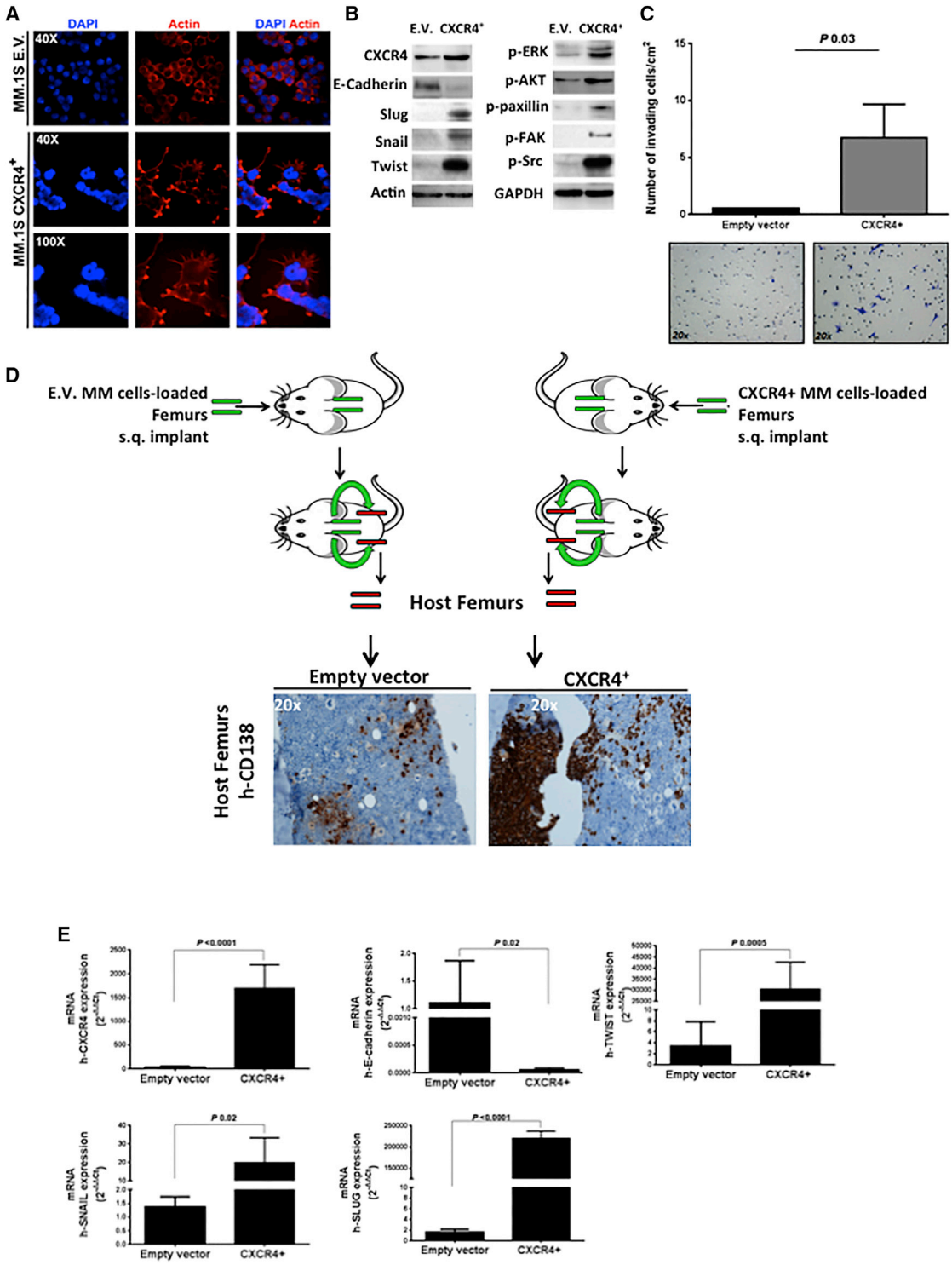

Figure 3. CXCR4 Mediates Acquisition of EMT-like Features in MM Cells In Vitro and In Vivo

(A) CXCR4-overexpressing MM.1S cells (MM.1S CXCR4+) present with an EMT-like phenotype compared to empty vector (EV)-infected cells used as control, as shown by confocal microscopy. Anti-actin Ab and DAPI were used to stain cytoplasm and nuclei, respectively. (40× and 100× magnifications are provided).

(B) Protein cell lysates were obtained from CXCR4+ MM.1S cells present with modulation of EMT-related proteins, together with upregulation of pro-survival- and migration/adhesion-related proteins compared to EV-infected cells used as control.

(C) CXCR4+ MM.1S cells display enhanced invasive properties compared to EV-infected cells used as control. Error bars indicate SD.

(legend continued on next page)

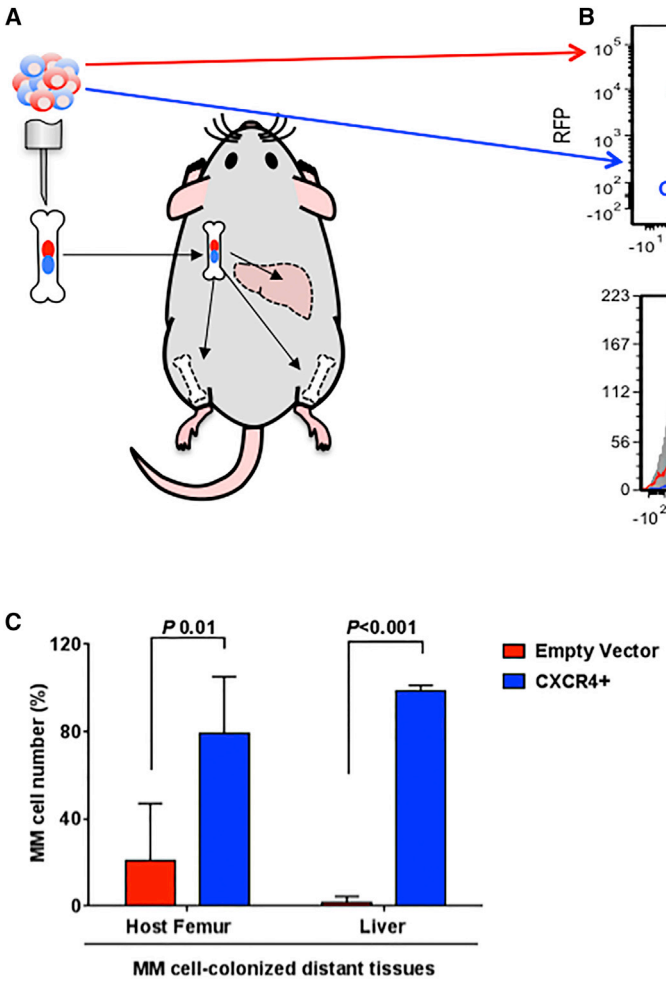

Figure 4. CXCR4 Overexpression Enhances MM Cell Ability to Disseminate to Medullary and Extra-Medullary Sites

(A) Schematic diagram of SCID-murine experiment. Four mice for each group were used. CXCR4-overexpressing (CXCR4/OE) MM cells carrying BFP and EV-transfected cells carrying RFP were used.

(B) Flow-cytometry analysis of the injected cell mixtures, showing equal distribution between the CXCR4/OE and the EV cells. CXCR4 expression of the cell populations was analyzed by gating BFP^+ or RFP^+ fractions.

(C) Number of CXCR4/OE and EV MM cells that colonized the host bone and the liver was quantified by flow cytometry. Error bars indicate SD.

upregulation and E-cadherin downregulation, when CXCR4 was overexpressed (Figures S3B and S3C).

CXCR4 Leads to Enhanced In Vivo Dissemination and Development of EMD

We first used an in vivo xenograft model of MM cell dissemination (Roccaro et al., 2014): MM cells, either CXCR4/OE or EV-infected (control), were loaded into femurs and implanted subcutaneously into recipient mice. CXCR4/OE cells presented with a higher ability to metastasize from bone to bone compared to control cells, as confirmed by using both immunohistochemistry and quantification by flow cytometry in harvested host femurs (Figures 3D and S4A). CXCR4 overexpression was confirmed ex vivo on cells harvested from the host femur. Importantly, lower expression of human (h)-E-cadherin, together with higher mRNA expression of h-Twist, h-Snail, and h-Slug, was confirmed within the BM of the host femur (Figure 3E). Taken together, these observations further confirm that CXCR4 upregulates EMT-like transcription factors, leading to enhanced cell dissemination in vivo.

We further investigated whether CXCR4 can enhance EMD development by performing an in vivo competition assay: MM cells, either blue fluorescent protein $(BFP)^+$/CXCR4/OE or red fluorescent protein $(RFP)^+$/EV infected (control), were mixed in equal numbers and inoculated in syngeneic femurs that were transplanted unilaterally in the dorsum of mice (Figures 4A and 4B). We observed a significantly higher dissemination of CXCR4/OE MM cells to the liver tissue (EMD) compared to EV-infected MM cells used as control (Figure 4C), indicating a strong propensity of CXCR4/OE cells to disseminate to the liver, thus leading to EMD.

CXCR4 Silencing Leads to Reduced MM BM Homing, Tumor Growth, and Enhanced Survival

To corroborate the functional relevance of CXCR4 in supporting MM cell dissemination, CXCR4 loss-of-function studies were performed (Figure 5A). CXCR4 knockdown led to significant inhibition of MM cell homing to the BM, as shown by using intravital confocal microscopy (Figure 5B), together with inhibited MM tumor growth in vivo, as shown by using bioluminescence imaging (Figures 5C and 5D). Importantly, prolonged survival was documented in mice injected with CXCR4-silenced MM cells compared to control mice injected with scramble probe-infected MM cells (Figure 5E). Confirmation of CXCR4 k.d. was performed ex vivo by using qRT-PCR on BM cells obtained from harvested femurs (Figure 5F).

(D) Bone chips were loaded with either CXCR4+ MM.1S or EV-infected MM.1S and implanted subcutaneously into SCID/Bg-recipient mice (n = 5/group). One host femur was harvested and used for immunohistochemistry using anti-human CD138 for detecting metastasized MM.1S cells.

(E) Higher mRNA levels of CXCR4, Twist, Snail, and Slug, together with lower mRNA levels of E-cadherin, were observed in BM cells obtained from the host femurs of mice implanted with CXCR4+-loaded femurs compared to those where EV-infected cells were used. Error bars indicate SD.

p indicates p value. Average of experiments performed in triplicate is shown.

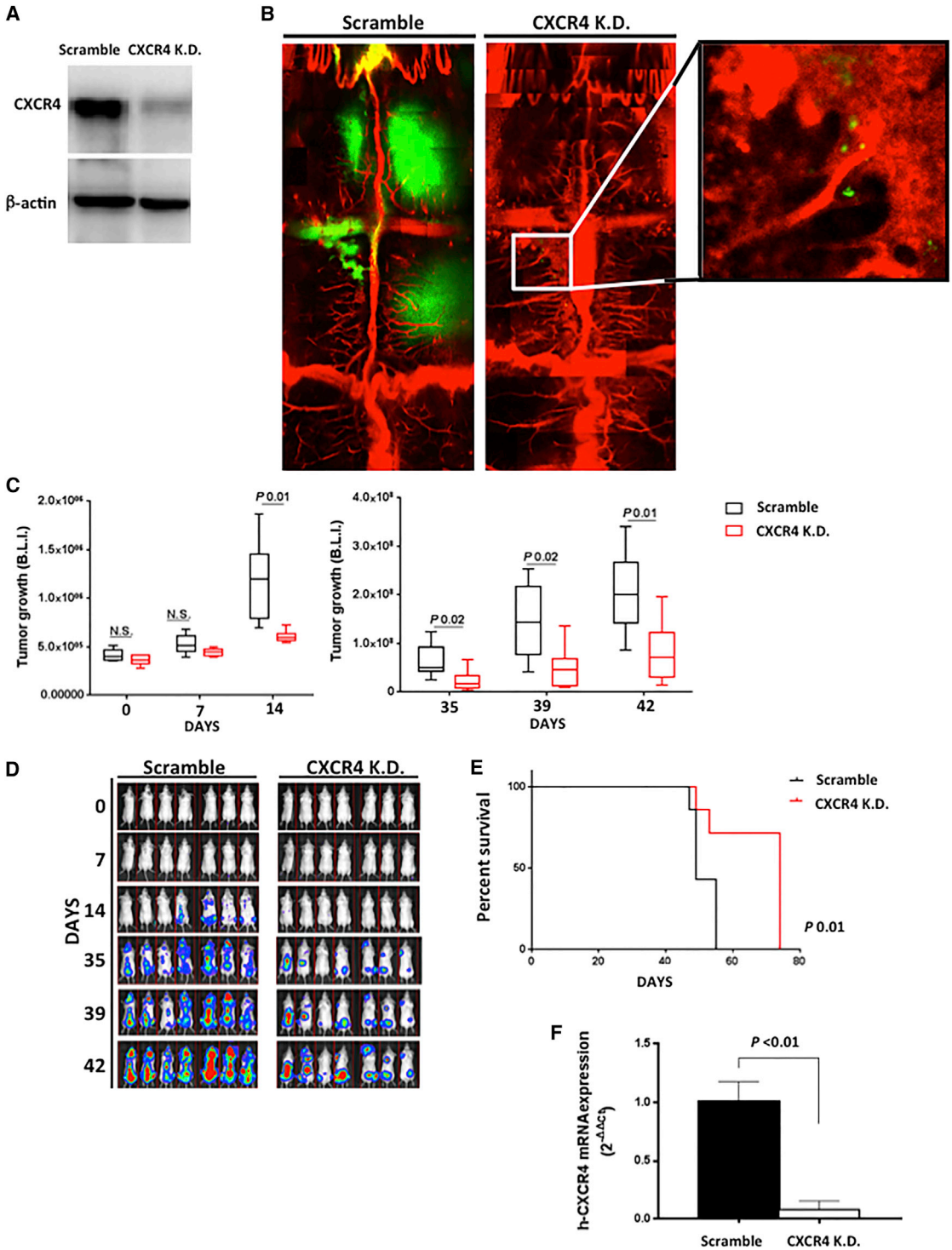

Figure 5. CXCR4-Silenced MM Cells Present with Reduced Homing, Tumor Growth In Vivo and Improved Survival

(A) Validation of CXCR silencing at protein level by western blot on CXCR4 K.D. MM cells as compared to scramble cells.

(B) CXCR4 silencing in MM cells led to inhibited MM cell homing to the bone marrow, as shown by using intravital confocal microscopy (day 34; GFP^+ MM cells, green color; Evans Blue positive-blood vessels, red color). High-resolution images with cellular detail were obtained through the intact mouse skull at depths of up to 250 μm from the surface of the skull using a 10× 0.45NA Plan-Apo objective (Carl Zeiss) and assembled together to generate a final image that depicts the whole bone marrow.

(C and D) SCID/Bg mice were injected with either CXCR4-silenced MM cells or scramble probe-infected cells (n = 7/group). Detection of tumor growth was performed by measuring bioluminescence imaging (BLI) intensity at different time points post-MM cell injection (days: 7; 14; 35; 39; and 42). CXCR4 silencing in MM cells led to inhibited MM tumor growth in vivo.

(legend continued on next page)

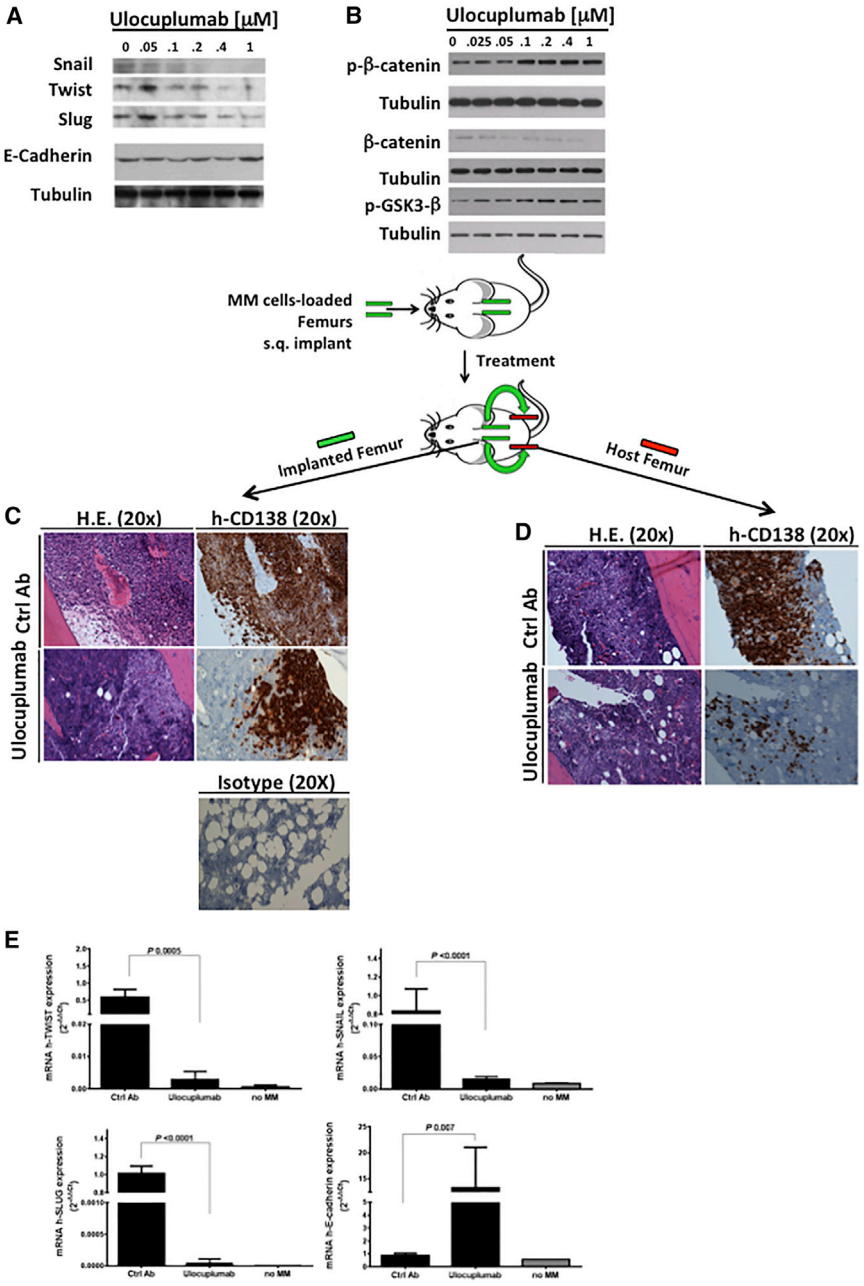

Figure 6. Ulocuplumab Inhibits the EMT Phenotype Acquisition in MM Cells Both In Vitro and In Vivo

(A and B) MM.1S cells were cultured in presence or absence of ulocuplumab (0.025–1 μM; 6 hr). MM.1S cells were then harvested, and cell lysates were subjected to western blot using anti-p-β-catenin, -β-catenin, -p-GSK3-β, -tubulin, -Snail, -Twist, -Slug, and -E-cadherin antibodies. Adjusted band intensity for each protein normalized to the relative loading control is provided within Figures S5A and S5B and expressed as fold of control (control corresponds to untreated cells).

(C and D) Bone chips from donor mice were loaded with CXCR4+ MM.1S and implanted subcutaneously into SCID/Bg-recipient mice. Mice were treated with either control Ab or ulocuplumab (n = 5/group; 10 mg/kg; i.p.; 4× to 5×/week). Ulocuplumab led to inhibited MM cell growth within the implanted bone (implanted bone is shown in C), together with inhibited ability of MM cells to metastatize from bone to bone (host bone is shown in D).

(E) The ability of ulocuplumab to modulate EMT was demonstrated ex vivo: decreased mRNA levels of Twist, Snail, and Slug, together with increased mRNA levels of E-cadherin, were observed in BM cells obtained from the host femurs of ulocuplumab-treated mice. No MM cell-injected mice were used as control. p indicates p value. Average of experiments performed in triplicate is shown. Error bars indicate SD.

CXCR4 Inhibition by a Selective Monoclonal Antibody, Ulocuplumab, Leads to Reduced MM Cell Dissemination Supported by EMT Inhibition

We further confirmed that CXCR4 is a critical regulator of EMT activation by evaluating the effects of the selective monoclonal antibody anti-CXCR4 (ulocuplumab) on the modulation of tumor cell dissemination and EMT, using clinically achievable concentrations (Kuhne et al., 2013). MM cells were exposed to increasing concentrations of the anti-CXCR4 monoclonal antibody, ulocuplumab. Ulocuplumab led to the regulation of EMT transcription factors including Snail, Twist, Slug, and E-cadherin (Figures 6A and S5A). Ulocuplumab also led to up-regulation of p-GSK3β and p-β-catenin, responsible for β-catenin degradation (Figures 6B and S5B). β-catenin is considered a marker of EMT in the context of embryonic development, fibrosis, and tumor progression (Brabletz et al., 1998; Kalluri and Neilson, 2003; Medici et al., 2006) and has been shown to modulate gene expression related to EMT, such as Snail. Our findings therefore suggest a possible role of CXCR4 in mediating acquisition of the EMT phenotype through β-catenin modulation.

To further investigate whether CXCR4 blockade may lead to an inhibition of MM cell dissemination to BM niches, we tested

(E) Kaplan-Meier curve showing prolonged survival in CXCR4 K.D. cell-injected mice versus scramble probe cell-injected mice (n = 7/group). p indicates p value (log rank test).

(F) Detection of human CXCR4 level has been performed by qRT-PCR (ΔΔCt method) on cells isolated ex vivo from the bone marrow femurs. p indicates p value. Error bars indicate SD.

Bars indicate SD. p indicates p value.

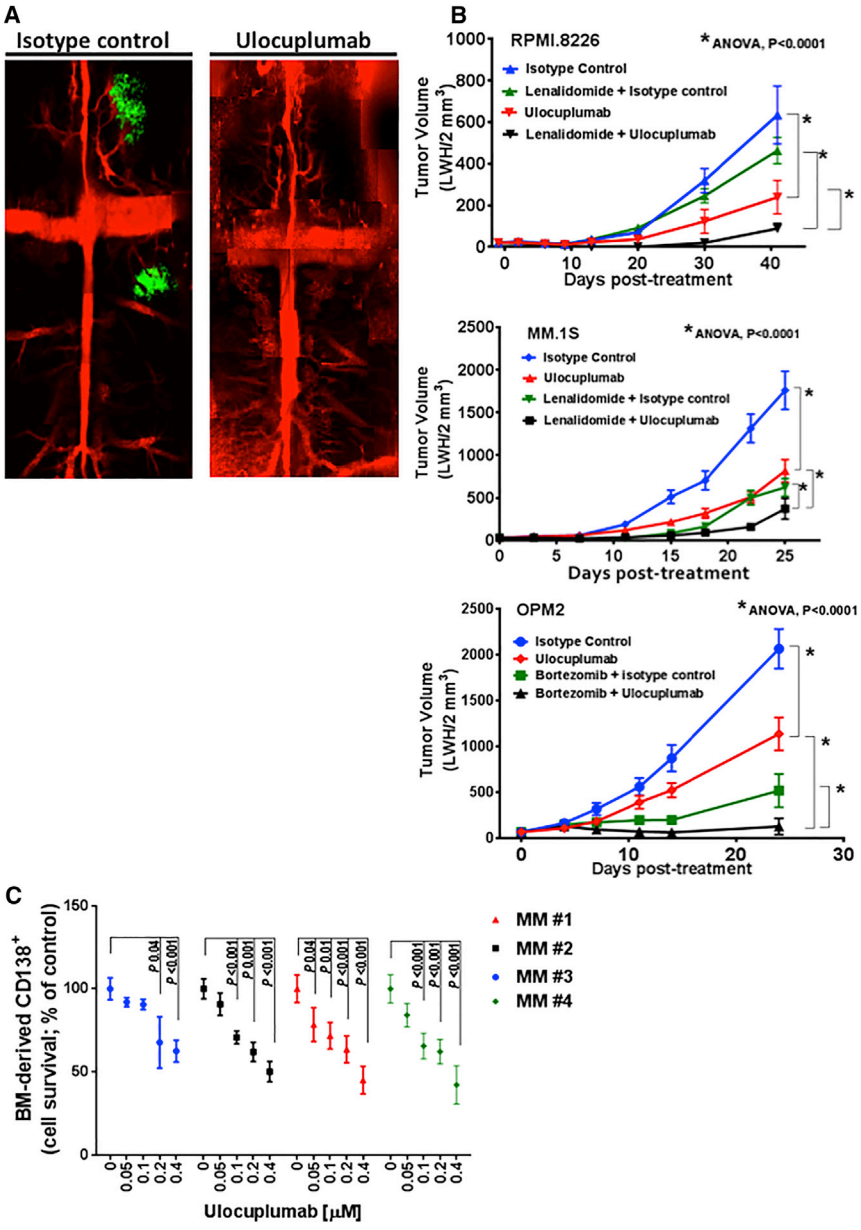

Figure 7. Ulocuplumab Exerts Anti-MM Activity, Either as Single Agent or in Combinatory Regimens In Vivo, and Induces Toxicity on Primary MM Cells

(A) SCID/Bg mice were injected with 5 × 10^6 MM.1S-GFP$^+$/Luc$^+$ cells i.v. and treated with ulocuplumab (10 mg/kg; 3× to 4×/week; i.p.) or isotype control antibody (30 mg/kg; 3× to 4×/week; i.p.). Ulocuplumab led to inhibited MM cell homing to the BM, as shown by using intravital confocal microscopy at the 3rd week. (GFP$^+$ MM cells, green color; Evans-Blue-positive blood vessels, red color). High-resolution images with cellular detail were obtained through the intact mouse skull at depths of up to 250 μm from the surface of the skull using a 10× 0.45NA Plan-Apo objective (Carl Zeiss) and assembled together to generate a final image that depicts the whole bone marrow.

(B) SCID mice were implanted with RPMI-8226, MM.1S cells and treated with ulocuplumab (10 mg/kg; 3× to 4×/week; i.p.), isotype control antibody (30 mg/kg; 3× to 4×/week; i.p.), or lenalidomide alone (50 mg/kg; daily; i.p.) or in combination with ulocuplumab, starting 8 days post-implantation (n = 8/group). Similarly, SCID mice were implanted with OPM-2 cells s.q. and treated with ulocuplumab (10 mg/kg; 3× to 4×/week; i.p.), isotype control antibody (30 mg/kg; 3× to 4×/week; i.p.), bortezomib alone (0.8 mg/kg; 2×/week), or in combination with ulocuplumab, starting 14 days post-implantation.

(C) BM-derived primary CD138+ cells were cultured in presence or absence of ulocuplumab (50–400 nM; 48 hr). Cell toxicity was performed by using MTT. Ulocuplumab exerted anti-MM activity against primary MM cells. Error bars indicate SD.

the effect of ulocuplumab on tumor dissemination in vivo, using clinically achievable concentrations (Kuhne et al., 2013). Ulocuplumab exerted an anti-MM activity in situ, within the s.q. implanted bones (Figure 6C), and also reduced MM cell dissemination/metastasis from the implanted bone to the host bone (Figures 6D and S6A). We next examined whether ulocuplumab modulated EMT-related gene expression in the MM cells metastasized to the host bones. We found that higher mRNA expression of h-E-cadherin, together with reduced mRNA expression of h-Twist, h-Snail, and h-Slug was found in BM cells harvested from the host bones of mice treated with ulocuplumab. These results confirm that the reduced MM cell dissemination to the host bone is a result of the combinatory effect of ulocuplumab-dependent modulation of EMT in addition to ulocuplumab-dependent modulation of tumor growth within the primary implanted bone. Non-MM-harboring mice were used as controls (Figure 6E).

To further demonstrate that CXCR4 inhibition may lead to inhibited MM cell homing to the BM, ulocuplumab was tested in vivo. MM.1S GFP+/Luc+ cells were injected i.v. into SCID/Bg mice and treated with either control Ab or ulocuplumab. Ulocuplumab-treated mice presented with reduced BM homing, as shown by intravital confocal microscopy (Figure 7A). In addition, using s.q. xenograft models, mice were treated with control Ab or ulocuplumab: in all the three models in which three different MM cell lines were used, ulocuplumab showed significant anti-MM activity compared to control Ab-treated mice. In addition to the anti-MM effect of ulocuplumab used as single agent, a more-significant MM tumor growth inhibition was observed in vivo when ulocuplumab was used in combinatory regimens with lenalidomide and bortezomib (Figure 7B). We next validated the effect of ulocuplumab on targeting patient BM-derived MM cells, showing induction of toxicity on primary MM cells exposed to increasing doses of ulocuplumab (Figure 7C). The observed ulocuplumab-mediated anti-MM activity

in vivo was also supported by the demonstration of ulocuplumab-dependent inhibition of MM cell proliferation in the context of primary BM mesenchymal stromal (BM-MSC) cells, in vitro (Figure S7A). We further corroborated these findings at protein levels: primary MM BM-MSCs were cultured in the presence of MM cells exposed to increasing concentrations of ulocuplumab. We demonstrated that ulocuplumab inhibited the BM-MSC-dependent upregulation of p-ERK, p-Akt, and p-Src in MM cells (Figure S7B). Importantly, possible mechanisms of ulocuplumab-induced MM cell apoptosis were studied, showing the ability of ulocuplumab to target MM cells in a caspase-dependent manner, as demonstrated by induced cleavage of both caspase-9 and PARP (Figure S7C).

DISCUSSION

CXCR4 has been considered a hallmark regulator of tumor metastasis as demonstrated both in solid tumors (Müller et al., 2001) and in hematological malignancies such as MM (Azab et al., 2012a; Möller et al., 2003), AML (Brault et al., 2014; Burger et al., 2003), and ALL (Juarez et al., 2009). However, none of these studies have previously implicated CXCR4 in the promotion of MM growth to EMD sites. The presence of multiple lytic lesions is one of the main clinical features of patients with active MM, thus suggesting the ability of clonal plasma cells to disseminate from bone to bone (Ghobrial, 2012; Kyle and Rajkumar, 2008). The BM-homing process of MM cells has been shown to be supported by the activation of the CXCR4/CXCL12 axis (Alsayed et al., 2007; Roccaro et al., 2014). Recent evidence supports that CXCL12 is essential in favoring a pro-metastatic BM niche in MM, as well as in bone metastatic solid tumors, including lung, gastric, medullary thyroid, renal, and prostate carcinomas (Roccaro et al., 2014). Type 3 epithelial-to-mesenchymal transition (EMT) represents one of the main features of metastatic solid tumor cells, where malignant epithelial cells display the ability to leave the primary tumor nodule, migrate to distant tissue sites, and create a secondary metastatic tumor nodule (Kalluri and Weinberg, 2009; Yang and Weinberg, 2008). In a small fraction of MM patients, plasma cells are capable of infiltrating EMD sites including liver, CNS, lungs/pleural fluid, and subcutaneous areas (Weinstock and Ghobrial, 2013). These patients are usually refractory to therapeutic agents and have a poor prognosis. This indicates that there is an urgent need for understanding the molecular mechanisms responsible for MM cell dissemination to EMD sites, thus potentially allowing for the development of better therapeutic modalities that target this unique subset of patients.

Previous observations have demonstrated that induction of the EMT phenotype leads to enhanced CXCR4 expression in epithelial tumors (Jung et al., 2013; Müller et al., 2001). However, no prior studies have shown that EMT may occur in hematologic malignancies, such as MM, and that CXCR4 can possibly modulate the acquisition of an EMT-like phenotype in the context of MM.

Here, we have generated BM- and EMD (liver)-prone MM clones by serial in vivo selection using MM xenograft mouse models, defined a significant EMT-related mRNA signature in both clones as compared to the parental MM cells, and confirmed the presence of CXCR4 at protein level in both the BM- and the EMD-prone clones. Importantly, an EMT mRNA signature was significantly enriched in MM patients with advanced disease, according to ISS (Greipp et al., 2005). By interrogating whether the CXCR4 levels may affect the EMT signature, we stratified primary BM-derived plasma cells obtained from MM patients according to their CXCR4 expression and found that patient-derived plasma cells with high CXCR4 expression present with significant enrichment of EMT-related pathways compared to those obtained from patients with low CXCR4 expression, thus suggesting a potential role for CXCR4 in facilitating the acquisition of an EMT phenotype in MM. We therefore interrogated whether CXCR4 may favor the ability of MM cells to disseminate from bone to bone or to extra-medullary sites, such as the liver, by modulating their EMT phenotype, independently from the functional role of the CXCR4/CXCL12 axis. Our findings show that CXCR4 gain of function exerts a pro-EMT-like phenotype in MM cells, with a higher degree of cellular invasion and metastasis, as shown both in vivo and in vitro, leading to MM disease progression. Importantly, the presence of an EMT signature was also defined and confirmed at the transcriptome level in liver-metastasizing MM clones. In contrast, CXCR4-silenced MM cells presented with reduced tumor growth in vivo together with enhanced survival. Importantly, the novel monoclonal anti-CXCR4 antibody exerted a dual effect against MM cells, as shown by inhibition of EMT both in vivo and in vitro, supported by reduced cell survival and induced cell apoptosis. Therefore, our data support the activity of CXCR4 inhibitors such as ulocuplumab in regulating tumor cell dissemination and metastasis through the inhibition of EMT transcriptional regulation.

A previous study had shown that bortezomib-resistant murine cell lines show reduced expression level of CXCR4 compared to the bortezomib-sensitive counterpart (Stessman et al., 2013), and this predicted poor survival in MM patients treated with the proteasome inhibitor. The bortezomib-resistant murine MM subclones may present with different genomic aberrations or changes at transcriptome level, compared to the bortezomib-sensitive murine MM subclones, and that may explain the results in this report. However, recent clinical studies do not support an increase in the incidence of EMD development post-bortezomib therapy (Weinstock et al., 2015). Therefore, we hypothesize that specific MM cell subclones may have differences in CXCR4 expression; it could also be postulated that a small subclone within the BM that has specific mutations or copy number alterations is more "fit" and capable of metastasis with specific tropism to EMD sites. Alternatively, subclones that disseminate to the BM or to EMD sites may upregulate CXCR4 by epigenetic alterations or hypoxia-driven upregulation of CXCR4 to allow for the proliferation and survival of these cells in a new host environment. Further studies are, therefore, necessary to define these potential mechanisms that lead to upregulation of CXCR4.

Taken together, these studies indicate that EMD development and cell dissemination and metastasis in MM is regulated by an upregulation of EMT-like transcriptional activity that leads to higher CXCR4 expression. Moreover, specific inhibition of CXCR4 by a monoclonal antibody can serve as a therapeutic

target of EMT activation and inhibition of tumor dissemination in MM specifically in EMD.

EXPERIMENTAL PROCEDURES

Cells

Primary BM-MSCs were obtained from MM patients. BM mononuclear cells were isolated using Ficoll gradient centrifugation. Primary plasma cells were isolated using microbead (CD138)-positive selection. The remaining population (CD138 negative) was cultured and selected in plastic flasks and used at the third to fourth passage. Following with previous reports and International Society for Cellular Therapy recommendations (Dominici et al., 2006; Garayoa et al., 2009; Roccaro et al., 2013), BM-MSCs were devoid of hematopoietic cells (CD34−, CD138−, CD45−, and CD14−) and positive for the remaining markers (CD73+, CD90+, CD105+, and CD106+), indicating their multipotent mesenchymal stromal cell phenotype. Approval for these studies was obtained from the Dana-Farber Cancer Institute Institutional Review Board. Informed consent was obtained from all patients and healthy volunteers in accordance with the Declaration of Helsinki protocol. The luciferase (luc)-expressing MM.1S-GFP/luc cell lines were generated by retroviral transduction with the pGC-gfp/luc vector (kind gift of Dr. A. Kung, Dana-Farber Cancer Institute). MM.1S, RPMI.8226, and IM9 cell lines were purchased from ATCC; OPM2 cells were purchased from DMSZ. Primary MM-BM-derived CD138+ cells were purified using CD138-microbeads (Miltenyi Biotech).

Development of BM- and EMD-Prone MM Clones

BM-prone and EMD-prone MM cell lines were developed by serial in vivo selection. A schematic representation of the experimental procedure is provided in Figure S1. Briefly, a total of 5×10^6 GFP^+MM.1S cells were injected into mice by intravenous injection. After hind-limb paralysis development, MM cells were harvested from either BM or liver from euthanized mice. To harvest BM engrafted MM cells, femurs and tibias were resected and BM mononuclear cells were collected. To harvest liver engrafted human MM cells, whole liver was resected under sterile conditions. The resected livers were minced with sterile razor blades and placed in RPMI 1640 media supplemented with collagenase/Dispase/DNase I enzyme mixture (Roche Diagnostics). Samples were incubated at 37°C for 1 hr with gentle shaking. After enzyme digestion, cells were washed three times with RPMI 1640 media and underwent Ficoll density gradient centrifugation to remove dead cells and debris. Total number of human MM cells was calculated by counting GFP+ cells under an epi-fluorescent microscope using hemocytometer. Cells were resuspended in culture medium and allowed to grow. GFP+ cells were sorted for further propagation in culture or for inoculation into new mice. After the first in vivo selection, MM cells harvested from different mice were pooled, and the resulting cell populations were subjected to the second round and third rounds of in vivo selection.

Fluorescent Imaging on Transparentized Mice

Mice injected with BM-prone or EMD-prone myeloma cells were observed for their tumor localization after transparentizing the mice using "clear, unobstructed brain imaging cocktails and computational analysis" (CUBIC) reagent as previously described (Susaki et al., 2014). Briefly, mice were injected with 0.1 ml of 1 mg/ml DyLight594-labeled Lycopersicon Esculentum Lectin (Vector Laboratories) for blood vessel staining. After anesthesia with isoflurane, the mice were transcardially perfused with PBS, 4% (w/v) paraformaldehyde, and CUBIC-1 reagent via heart left ventricle. Mice were subsequently immersed in CUBIC-1 reagent for 5 days and further immersed in CUBIC-2 reagent for additional 5 days. Lower magnification images were obtained using an OV100 whole-mouse imaging system (Olympus). Images were acquired with 0.13×, 0.27×, and 0.56× objective lenses. All data were taken with a monochrome digital charge-coupled device (CCD) camera (F-View II; Olympus Soft Imaging Solutions). To observe the tumors with high magnification, liver, femurs, and tibias were resected from transparentized mice and observed using a confocal microscopy (FV-1000; Olympus). Images were acquired using a 30× silicone immersion objective lens (NA 1.05). 3D reconstruction was performed from z stack images using Volocity software (PerkinElmer).

Reagents

Ulocuplumab and the control human IgG4 isotype control were obtained from Bristol-Myers Squibb. Bortezomib and lenalidomide were obtained from Selleck Chemicals.

Immunohistochemistry and Immunofluorescence

Autopsy specimens of synchronous secondary extramedullary MM sites were analyzed for the expression of CD138 and CXCR4. Murine BM tissues (femurs) were analyzed for the expression of human CD138 and stained with hematoxylin-eosin. Images were taken using Nikon Eclipse 80i microscope (objectives 20× and 100×). Immunofluorescence imaging was performed on CXCR4-overexpressing MM cells for evaluating actin cytoskeleton reorganization, using a confocal microscope (Nikon TE2000-E; objectives 40× and 100×). DAPI was used as nuclear staining. Anti-actin Alexa Fluor 594 conjugated was used (Cell Signaling). Images were taken using the Hamamatsu OrcaER camera and the NIS-Element software. Image J was used to merge the two different channels.

Immunoblotting

Cells were harvested and lysed using lysis buffer (Cell Signaling Technology) supplemented with 5 mM NaF, 2 mM Na_3VO_4, 1 mM PMSF (polymethylsulfonyl fluoride), 5 μg/ml leupeptin, and 5 μg/ml aprotinin. Whole-cell lysates were subjected to SDS-PAGE and transferred to polyvinylidene fluoride (PVDF) membrane (Bio-Rad). The antibodies used for immunoblotting included anti-CXCR4, -E-cadherin, -N-cadherin, -Slug, -Snail, -Twist, phosphor (p)-ERK, -p-Akt, -p-paxillin, -p-Src, p-β-catenin, -β-catenin, -p-GSK3-β, -caspase-9, -PARP, -GAPDH, -tubulin, and -actin antibodies (Cell Signal). Protein band quantification was obtained using Image J, as previously described (Kovaleva et al., 2012).

In Vitro Studies

DNA synthesis was measured by [^{3}H]-thymidine ([^{3}H]-TdR; PerkinElmer) uptake, or MTS, as previously described (Roccaro et al., 2010; Sacco et al., 2011). Cell toxicity has been evaluated by measuring 3-(4,5-dimethylthiazol-2-yl)-2,5-diphenyltetrazolium bromide (MTT; Chemicon International), as described (Azab et al., 2012b; Roccaro et al., 2010; Sacco et al., 2011). Invasion assay was assessed using a Matrigel invasion chamber assay (Corning). Cell migration was determined using the transwell migration assay (Costar), as previously described (Azab et al., 2012a).

In Vivo Studies

Intravital confocal microscopy was performed as previously reported (Colmone et al., 2008; Roccaro et al., 2013) using a Zeiss 710 confocal system (Carl Zeiss) on an upright Examiner stand with a custom stage. Briefly, a skin flap was made in the scalp of the mice to expose the underlying dorsal skull surface. High-resolution images with cellular detail were obtained through the intact mouse skull at depths of up to 250 μm from the surface of the skull using a 10× 0.45NA Plan-Apo objective (Carl Zeiss) and assembled together to generate a final image that depicts the whole bone marrow. Multiple imaging depths were acquired, and a maximum intensity z projection was performed to merge the images. GFP was excited with the 488 nm line on an argon laser. Blood vessels were imaged using Evans Blue (Sigma-Aldrich) excited with a 633 nm laser. Emission signals were collected by using the Zeiss internal confocal Quasar detectors.

In vivo tumor growth has been assessed by using in vivo bioluminescence imaging. Mice were injected with 75 mg/kg of Luciferin (Xenogen), and tumor growth was detected by bioluminescence 3 min after the injection, using Xenogen In Vivo Imaging System (Caliper Life Sciences), as previously reported (Roccaro et al., 2009). The in vivo MM metastasis model was performed, as previously reported (Roccaro et al., 2014). Briefly, bone chips were loaded with human (GFP^+ MM.1S) MM cells (2×10^6 cells/bone). Two bones were implanted subcutaneously into SCID/Bg mice (n = 5/group). Mice received either isotype control antibody or ulocuplumab (intra-peritoneal [i.p.]; 10 mg/kg; 3× to 4×/week). Mice were euthanized once signs or limb paralysis were evident. MM cells have been harvested from one host femur and evaluated by flow cytometry for GFP/human CD138 positivity. The remaining host femur has been used for immunohistochemistry using human anti-CD138 for detecting metastasized MM.1S cells. Six-week-old female SCID-beige mice (Taconic) were

treated, monitored, and sacrificed in accordance with approved protocol of the Dana-Farber Cancer Institute Animal Care and Use Committee.

MM Xenograft s.q. Models

SCID mice were subcutaneously implanted with 10 million RPMI-8226, MM.1S, or OPM-2 cells in 0.1 ml PBS and 0.1 ml Matrigel, as previously described (Zhang et al., 2014). One day prior to dosing, mice were randomized into groups of eight mice each according to tumor volume (L × W × H/2). Post-implantation, mice were dosed with ulocuplumab (10 mg/kg; 3× to 4×/week; i.p.), human IgG4 isotype (30 mg/kg; 3× to 4×/week; i.p.), bortezomib (0.8 mg/kg; 2×/week; i.p.), or Revlimid (50 mg/kg; daily; i.p.). Tumors and body weights were measured twice weekly. Tumors were measured in three dimensions with a Fowler Electronic Digital Caliper (model 62379-531; Fred V. Fowler), and data were electronically recorded using StudyDirector software from Studylog Systems. Animals were checked daily for postural, grooming, and respiratory changes, as well as lethargy. Mice were euthanized when the tumors reached the 2,000 mm^3 endpoint or appeared ulcerated. All antibody doses were well tolerated, and no body weight losses were observed.

CXCR4 Gain and Loss of Function

CXCR4 was silenced in MM.1S cells using shRNAs and lentivirus-mediated infection; scramble probe has been used as control (G9 clone; TRCN0000256866; Broad Institute RNAi Consortium), according to manufacturer's specifications. Transduction efficiency was performed by using qRT-PCR and western blot (Livak and Schmittgen, 2001). Overexpression of CXCR4 was obtained in MM.1S and RPMI.8226 cells using precision LentiORF/CXCR4 ($CXCR4^+$) or EV used as control (Thermo Scientific). Overexpression efficiency was performed by using qRT-PCR and western blot (Livak and Schmittgen, 2001).

mRNA Studies

We utilized a public MM gene expression data set GSE24080 to explore the pathways potentially regulated by CXCR4. We ranked all 577 MM samples by their normalized CXCR4 expression levels and compared gene expression between top 100 samples with highest CXCR4 expression and top 100 samples with lowest CXCR4 expression. Gene set enrichment analysis (GSEA) was used to identify significantly enriched pathways (Subramanian et al., 2005). Gene sets were downloaded from the Broad Institute's MSigDB (http://www.broadinstitute.org/gsea/index.jsp).

RNA Sequencing Analysis

Total RNA was isolated from EMD-prone and BM-prone cell lines using RNeasy Mini kit (QIAGEN). During isolation step, RNA was treated with DNase I according to the manufacturer's protocol. For RNA sequencing, poly-A selection and cDNA synthesis were performed, followed by library preparation using Illumina TruSeq RNA Sample Prep Kit, sequencing (75-bp paired reads), and sample identification for quality control. We used Bcbio_nextgen (https://github.com/chapmanb/bcbio-nextgen/) to process the RNA-seq data. Briefly, cutadapt (https://github.com/marcelm/cutadapt/) was used to trim adapters, trimmed reads were aligned to human reference genome (*GRCh37*) with tophat2 (Kim et al., 2013), and read count for each gene was calculated by HT-seq (Anders et al., 2015). Genes with low expression (FPKM < 1 across all samples) were filtered out. GSEA was used to identify differentially expressed mRNA signatures, with false discovery rate (FDR) < 0.25 and p value < 0.05.

Statistics

The p values described in the in vitro assays are based on t tests (two-tailed; α 0.05). p values are provided for each figure. The average of experiments performed in triplicate is shown. The Kaplan-Meier curve was obtained using GraphPad Prism, and the p value was calculated based on log rank test.

ACCESSION NUMBERS

The accession numbers for the data reported in this paper are GEO: GSE68538, GEO: GSE24080, and GEO: GSE6477.

SUPPLEMENTAL INFORMATION

Supplemental Information includes seven figures and three tables and can be found with this article online at http://dx.doi.org/10.1016/j.celrep.2015.06.059.

AUTHOR CONTRIBUTIONS

A.M.R., Y.M., A.S., and I.M.G. conceived and designed the experiments and analyzed the data. A.M.R. wrote the manuscript. J.S. and S.M. performed bioinformatics analysis. Y.-T.T. provided primary MM samples. M. Chiarini, M. Cea, and S.G. performed myeloma in vitro studies. D.H., M.M., Y.M., Y.K., and I.S. performed myeloma in vivo studies. M.R.R. and Y.Z. performed in vivo confocal microscopy. Y.A. collected EMD samples. E.M. performed IHC studies. P.C., M.K., and C.P. provided ulocuplumab and isotype control reagents. M.K., P.C., F.M., and I.M.G. revised the manuscript.

ACKNOWLEDGMENTS

The following support is acknowledged: NIH/National Cancer Institute (RO1CA181683); The Leukemia & Lymphoma Society; and the Dana-Farber Cancer Institute Physical Sciences Oncology Center (NCI grant U54CA143798). M.K., P.C., and C.P. are employees at Bristol-Myers Squibb. I.M.G. is a member of the BMS advisory board and received research support.

Received: May 19, 2015
Revised: June 4, 2015
Accepted: June 16, 2015
Published: July 16, 2015

REFERENCES

Acloque, H., Adams, M.S., Fishwick, K., Bronner-Fraser, M., and Nieto, M.A. (2009). Epithelial-mesenchymal transitions: the importance of changing cell state in development and disease. J. Clin. Invest. *119*, 1438–1449.

Alsayed, Y., Ngo, H., Runnels, J., Leleu, X., Singha, U.K., Pitsillides, C.M., Spencer, J.A., Kimlinger, T., Ghobrial, J.M., Jia, X., et al. (2007). Mechanisms of regulation of CXCR4/SDF-1 (CXCL12)-dependent migration and homing in multiple myeloma. Blood *109*, 2708–2717.

Anders, S., Pyl, P.T., and Huber, W. (2015). HTSeq—a Python framework to work with high-throughput sequencing data. Bioinformatics *31*, 166–169.

Ansieau, S., Bastid, J., Doreau, A., Morel, A.P., Bouchet, B.P., Thomas, C., Fauvet, F., Puisieux, I., Doglioni, C., Piccinin, S., et al. (2008). Induction of EMT by twist proteins as a collateral effect of tumor-promoting inactivation of premature senescence. Cancer Cell *14*, 79–89.

Azab, A.K., Hu, J., Quang, P., Azab, F., Pitsillides, C., Awwad, R., Thompson, B., Maiso, P., Sun, J.D., Hart, C.P., et al. (2012a). Hypoxia promotes dissemination of multiple myeloma through acquisition of epithelial to mesenchymal transition-like features. Blood *119*, 5782–5794.

Azab, F., Azab, A.K., Maiso, P., Calimeri, T., Flores, L., Liu, Y., Quang, P., Roccaro, A.M., Sacco, A., Ngo, H.T., et al. (2012b). Eph-B2/ephrin-B2 interaction plays a major role in the adhesion and proliferation of Waldenstrom's macroglobulinemia. Clin. Cancer Res. *18*, 91–104.

Brabletz, T., Jung, A., Hermann, K., Günther, K., Hohenberger, W., and Kirchner, T. (1998). Nuclear overexpression of the oncoprotein beta-catenin in colorectal cancer is localized predominantly at the invasion front. Pathol. Res. Pract. *194*, 701–704.

Brabletz, T., Jung, A., Reu, S., Porzner, M., Hlubek, F., Kunz-Schughart, L.A., Knuechel, R., and Kirchner, T. (2001). Variable beta-catenin expression in colorectal cancers indicates tumor progression driven by the tumor environment. Proc. Natl. Acad. Sci. USA *98*, 10356–10361.

Brault, L., Rovó, A., Decker, S., Dierks, C., Tzankov, A., and Schwaller, J. (2014). CXCR4-SERINE339 regulates cellular adhesion, retention and

mobilization, and is a marker for poor prognosis in acute myeloid leukemia. Leukemia *28*, 566–576.

Burger, M., Glodek, A., Hartmann, T., Schmitt-Gräff, A., Silberstein, L.E., Fujii, N., Kipps, T.J., and Burger, J.A. (2003). Functional expression of CXCR4 (CD184) on small-cell lung cancer cells mediates migration, integrin activation, and adhesion to stromal cells. Oncogene *22*, 8093–8101.

Colmone, A., Amorim, M., Pontier, A.L., Wang, S., Jablonski, E., and Sipkins, D.A. (2008). Leukemic cells create bone marrow niches that disrupt the behavior of normal hematopoietic progenitor cells. Science *322*, 1861–1865.

Dominici, M., Le Blanc, K., Mueller, I., Slaper-Cortenbach, I., Marini, F., Krause, D., Deans, R., Keating, A., Prockop, Dj., and Horwitz, E. (2006). Minimal criteria for defining multipotent mesenchymal stromal cells. The International Society for Cellular Therapy position statement. Cytotherapy *8*, 315–317.

Garayoa, M., Garcia, J.L., Santamaria, C., Garcia-Gomez, A., Blanco, J.F., Pandiella, A., Hernández, J.M., Sanchez-Guijo, F.M., del Cañizo, M.C., Gutiérrez, N.C., and San Miguel, J.F. (2009). Mesenchymal stem cells from multiple myeloma patients display distinct genomic profile as compared with those from normal donors. Leukemia *23*, 1515–1527.

Ghobrial, I.M. (2012). Myeloma as a model for the process of metastasis: implications for therapy. Blood *120*, 20–30.

Greipp, P.R., San Miguel, J., Durie, B.G., Crowley, J.J., Barlogie, B., Bladé, J., Boccadoro, M., Child, J.A., Avet-Loiseau, H., Kyle, R.A., et al. (2005). International staging system for multiple myeloma. J. Clin. Oncol. *23*, 3412–3420.

Gupta, P.B., Mani, S., Yang, J., Hartwell, K., and Weinberg, R.A. (2005). The evolving portrait of cancer metastasis. Cold Spring Harb. Symp. Quant. Biol. *70*, 291–297.

Hanahan, D., and Weinberg, R.A. (2000). The hallmarks of cancer. Cell *100*, 57–70.

Juarez, J.G., Thien, M., Dela Pena, A., Baraz, R., Bradstock, K.F., and Bendall, L.J. (2009). CXCR4 mediates the homing of B cell progenitor acute lymphoblastic leukaemia cells to the bone marrow via activation of p38MAPK. Br. J. Haematol. *145*, 491–499.

Jung, Y., Kim, J.K., Shiozawa, Y., Wang, J., Mishra, A., Joseph, J., Berry, J.E., McGee, S., Lee, E., Sun, H., et al. (2013). Recruitment of mesenchymal stem cells into prostate tumours promotes metastasis. Nat. Commun. *4*, 1795.

Kalluri, R., and Neilson, E.G. (2003). Epithelial-mesenchymal transition and its implications for fibrosis. J. Clin. Invest. *112*, 1776–1784.

Kalluri, R., and Weinberg, R.A. (2009). The basics of epithelial-mesenchymal transition. J. Clin. Invest. *119*, 1420–1428.

Kim, D., Pertea, G., Trapnell, C., Pimentel, H., Kelley, R., and Salzberg, S.L. (2013). TopHat2: accurate alignment of transcriptomes in the presence of insertions, deletions and gene fusions. Genome Biol. *14*, R36.

Kovaleva, V., Mora, R., Park, Y.J., Plass, C., Chiramel, A.I., Bartenschlager, R., Döhner, H., Stilgenbauer, S., Pscherer, A., Lichter, P., and Seiffert, M. (2012). miRNA-130a targets ATG2B and DICER1 to inhibit autophagy and trigger killing of chronic lymphocytic leukemia cells. Cancer Res. *72*, 1763–1772.

Kuhne, M.R., Mulvey, T., Belanger, B., Chen, S., Pan, C., Chong, C., Cao, F., Niekro, W., Kempe, T., Henning, K.A., et al. (2013). BMS-936564/MDX-1338: a fully human anti-CXCR4 antibody induces apoptosis in vitro and shows antitumor activity in vivo in hematologic malignancies. Clin. Cancer Res. *19*, 357–366.

Kyle, R.A., and Rajkumar, S.V. (2008). Multiple myeloma. Blood *111*, 2962–2972.

Livak, K.J., and Schmittgen, T.D. (2001). Analysis of relative gene expression data using real-time quantitative PCR and the 2(-Delta Delta C(T)) Method. Methods *25*, 402–408.

Medici, D., Hay, E.D., and Goodenough, D.A. (2006). Cooperation between snail and LEF-1 transcription factors is essential for TGF-beta1-induced epithelial-mesenchymal transition. Mol. Biol. Cell *17*, 1871–1879.

Medici, D., Hay, E.D., and Olsen, B.R. (2008). Snail and Slug promote epithelial-mesenchymal transition through beta-catenin-T-cell factor-4-dependent expression of transforming growth factor-beta3. Mol. Biol. Cell *19*, 4875–4887.

Möller, C., Strömberg, T., Juremalm, M., Nilsson, K., and Nilsson, G. (2003). Expression and function of chemokine receptors in human multiple myeloma. Leukemia *17*, 203–210.

Müller, A., Homey, B., Soto, H., Ge, N., Catron, D., Buchanan, M.E., McClanahan, T., Murphy, E., Yuan, W., Wagner, S.N., et al. (2001). Involvement of chemokine receptors in breast cancer metastasis. Nature *410*, 50–56.

Okada, H., Danoff, T.M., Kalluri, R., and Neilson, E.G. (1997). Early role of Fsp1 in epithelial-mesenchymal transformation. Am. J. Physiol. *273*, F563–F574.

Orimo, A., Gupta, P.B., Sgroi, D.C., Arenzana-Seisdedos, F., Delaunay, T., Naeem, R., Carey, V.J., Richardson, A.L., and Weinberg, R.A. (2005). Stromal fibroblasts present in invasive human breast carcinomas promote tumor growth and angiogenesis through elevated SDF-1/CXCL12 secretion. Cell *121*, 335–348.

Oriol, A. (2011). Multiple myeloma with extramedullary disease. Adv. Ther. *28* (*Suppl 7*), 1–6.

Roccaro, A.M., Sacco, A., Thompson, B., Leleu, X., Azab, A.K., Azab, F., Runnels, J., Jia, X., Ngo, H.T., Melhem, M.R., et al. (2009). MicroRNAs 15a and 16 regulate tumor proliferation in multiple myeloma. Blood *113*, 6669–6680.

Roccaro, A.M., Sacco, A., Husu, E.N., Pitsillides, C., Vesole, S., Azab, A.K., Azab, F., Melhem, M., Ngo, H.T., Quang, P., et al. (2010). Dual targeting of the PI3K/Akt/mTOR pathway as an antitumor strategy in Waldenstrom macroglobulinemia. Blood *115*, 559–569.

Roccaro, A.M., Sacco, A., Maiso, P., Azab, A.K., Tai, Y.T., Reagan, M., Azab, F., Flores, L.M., Campigotto, F., Weller, E., et al. (2013). BM mesenchymal stromal cell-derived exosomes facilitate multiple myeloma progression. J. Clin. Invest. *123*, 1542–1555.

Roccaro, A.M., Sacco, A., Purschke, W.G., Moschetta, M., Buchner, K., Maasch, C., Zboralski, D., Zöllner, S., Vonhoff, S., Mishima, Y., et al. (2014). SDF-1 inhibition targets the bone marrow niche for cancer therapy. Cell Rep. *9*, 118–128.

Sacco, A., Aujay, M., Morgan, B., Azab, A.K., Maiso, P., Liu, Y., Zhang, Y., Azab, F., Ngo, H.T., Issa, G.C., et al. (2011). Carfilzomib-dependent selective inhibition of the chymotrypsin-like activity of the proteasome leads to antitumor activity in Waldenstrom's Macroglobulinemia. Clin. Cancer Res. *17*, 1753–1764.

Schioppa, T., Uranchimeg, B., Saccani, A., Biswas, S.K., Doni, A., Rapisarda, A., Bernasconi, S., Saccani, S., Nebuloni, M., Vago, L., et al. (2003). Regulation of the chemokine receptor CXCR4 by hypoxia. J. Exp. Med. *198*, 1391–1402.

Smit, M.A., and Peeper, D.S. (2008). Deregulating EMT and senescence: double impact by a single twist. Cancer Cell *14*, 5–7.

Stessman, H.A., Mansoor, A., Zhan, F., Janz, S., Linden, M.A., Baughn, L.B., and Van Ness, B. (2013). Reduced CXCR4 expression is associated with extramedullary disease in a mouse model of myeloma and predicts poor survival in multiple myeloma patients treated with bortezomib. Leukemia *27*, 2075–2077.

Subramanian, A., Tamayo, P., Mootha, V.K., Mukherjee, S., Ebert, B.L., Gillette, M.A., Paulovich, A., Pomeroy, S.L., Golub, T.R., Lander, E.S., and Mesirov, J.P. (2005). Gene set enrichment analysis: a knowledge-based approach for interpreting genome-wide expression profiles. Proc. Natl. Acad. Sci. USA *102*, 15545–15550.

Susaki, E.A., Tainaka, K., Perrin, D., Kishino, F., Tawara, T., Watanabe, T.M., Yokoyama, C., Onoe, H., Eguchi, M., Yamaguchi, S., et al. (2014). Whole-brain imaging with single-cell resolution using chemical cocktails and computational analysis. Cell *157*, 726–739.

Thiery, J.P. (2002). Epithelial-mesenchymal transitions in tumour progression. Nat. Rev. Cancer *2*, 442–454.

Varettoni, M., Corso, A., Pica, G., Mangiacavalli, S., Pascutto, C., and Lazzarino, M. (2010). Incidence, presenting features and outcome of extramedullary disease in multiple myeloma: a longitudinal study on 1003 consecutive patients. Ann. Oncol. *21*, 325–330.

Vićovac, L., and Aplin, J.D. (1996). Epithelial-mesenchymal transition during trophoblast differentiation. Acta Anat. (Basel) *156*, 202–216.

Weinstock, M., and Ghobrial, I.M. (2013). Extramedullary multiple myeloma. Leuk. Lymphoma *54*, 1135–1141.

Weinstock, M., Aljawai, Y., Morgan, E.A., Laubach, J., Gannon, M., Roccaro, A.M., Varga, C., Mitsiades, C.S., Paba-Prada, C., Schlossman, R., et al. (2015). Incidence and clinical features of extramedullary multiple myeloma in patients who underwent stem cell transplantation. Br. J. Haematol. *169*, 851–858.

Yagi, H., Tan, W., Dillenburg-Pilla, P., Armando, S., Amornphimoltham, P., Simaan, M., Weigert, R., Molinolo, A.A., Bouvier, M., and Gutkind, J.S. (2011). A synthetic biology approach reveals a CXCR4-G13-Rho signaling axis driving transendothelial migration of metastatic breast cancer cells. Sci. Signal. *4*, ra60.

Yang, J., and Weinberg, R.A. (2008). Epithelial-mesenchymal transition: at the crossroads of development and tumor metastasis. Dev. Cell *14*, 818–829.

Yang, J., Mani, S.A., and Weinberg, R.A. (2006). Exploring a new twist on tumor metastasis. Cancer Res. *66*, 4549–4552.

Zeisberg, E.M., Tarnavski, O., Zeisberg, M., Dorfman, A.L., McMullen, J.R., Gustafsson, E., Chandraker, A., Yuan, X., Pu, W.T., Roberts, A.B., et al. (2007a). Endothelial-to-mesenchymal transition contributes to cardiac fibrosis. Nat. Med. *13*, 952–961.

Zeisberg, M., Yang, C., Martino, M., Duncan, M.B., Rieder, F., Tanjore, H., and Kalluri, R. (2007b). Fibroblasts derive from hepatocytes in liver fibrosis via epithelial to mesenchymal transition. J. Biol. Chem. *282*, 23337–23347.

Zhang, Y., Moschetta, M., Huynh, D., Tai, Y.T., Zhang, Y., Zhang, W., Mishima, Y., Ring, J.E., Tam, W.F., Xu, Q., et al. (2014). Pyk2 promotes tumor progression in multiple myeloma. Blood *124*, 2675–2686.